Applied Geomatics
https://doi.org/10.1007/s12518-019-00258-7

ORIGINAL PAPER

Exploring the synergy between Landsat and ASAR towards improving thematic mapping accuracy of optical EO data

Alexander Cass[1] · George P. Petropoulos[2,3] · Konstantinos P. Ferentinos[4] · Andrew Pavlides[3] · Prashant K. Srivastava[5]

Received: 12 February 2019 / Accepted: 19 March 2019

Abstract

Earth Observation (EO) provides a unique means of obtaining information on land use/cover and of its changes, which is of key importance in many scientific and practical applications. EO data is already widely used, for example, in environmental practices or decision-making related to food availability and security. As such, it is imperative to examine the suitability of different EO datasets, including their synergies, in respect to their ability to create products and tools for such practices and to guide effectively such decisions. This work aims at exploring the added value of the synergistic use of optical and radar data (from the Landsat TM and Advanced Synthetic Aperture Radar (*ASAR*) sensors respectively). Such information can help towards improving the accuracy of land cover classifications from EO datasets. As a case study, the region of Wales in the UK has been used. Two classifications—one based on optical data alone and another one developed from the synergy of optical and RADAR datasets acquired nearly, concurrently were developed for the studied region. Evaluation of the derived land/use cover maps was performed on the basis of the confusion matrix using validation points derived from a Phase 1 habitat map of Wales. The results showed 15% increase in overall accuracy (84% from 69%) and kappa coefficient (0.81 from 0.65) using the synergistic approach over the scenario where only optical data were used in the classification. In addition, McNemar's test was used to assess the statistical significance of the obtained results. Results of this test provided further confirmed that the use of optical data synergistically with the radar data provides more accurate land use/cover maps in comparison with the use of optical data alone.

Keywords Landsat · ASAR · SAR · Land use/cover mapping · Object-based classification · Classification · Earth Observation · GIS

Introduction

Food security is a global issue Bao et al. (2018) and Food and Agriculture Organization of the United Nations (2012). The role of Earth Observation (EO) in the context of food security is significant and expanding with time and new data. For example, the European Monitoring Agricultural Resources Unit (MARS) is a project which aims to provide such information since 1988 European Space Agency (2013). Another such program, which operates on a larger scale, is the Copernicus Program. The latter is a joint collaboration between the European Commission (EC), European Space Agency (ESA), and the European Environment Agency (EEA). Such activities have provided scientific and technical support on European agriculture and food security policies based on data at national, regional, and continental scale, the likes of which have been used to inform the policy makers of the Common Agricultural Policy (CAP) (Joint Research Centre 2013).

✉ George P. Petropoulos
petropoulos.george@gmail.com

[1] Department of Geography and Earth Sciences, University of Aberystwyth, Wales SY23 3DB, UK

[2] Department of Soil & Water Resources, Institute of Industrial & Forage Crops, Hellenic Agricultural Organization (HAO) - "Demeter", Larisa, Greece

[3] School of Mineral Resources Engineering, Technical University of Crete, Crete, Greece

[4] Department of Agricultural Engineering, Institute of Soil & Water Resources, Hellenic Agricultural Organization "Demeter", Athens, Greece

[5] Institute of Environment and Sustainable Development and DST-Mahamana Centre for Excellence in Climate Change Research, Banaras Hindu University, Varanasi, India

Published online: 13 April 2019

A key input into the policy making of the EC and other such organizations is the information derived from EO data. ESA has long provided satellite-based data for global and regional applications linked to food security, such as forestry, agriculture, environmental protection, and urban management. This has been mainly achieved through the Copernicus program. The continual supply of reliable EO data and of relevant EO operational products can provide key information on the distribution of land use/land cover (LULC) changes, at a variety of scales. Such datasets can be analyzed to indicate changes due to anthropogenic activities, natural hazards, or even climate change as a whole. This data is a key input to environmental policy makers the world over.

In terms of providing more specific information for food security purposes, crop mapping has been extensively undertaken using optical imagery (Elatawneh et al. 2012; Lamine et al. 2018). Furthermore, the benefits of using EO data for this purpose have been widely demonstrated (Gómez et al. 2016 Zhu et al. 2012) and the importance of time series data for high-accuracy classification has been highlighted in several studies (e.g., Srivastava et al. 2012, 2015, 2016; Singh et al. 2014). However, an ever occurring problem with the use of optical satellite data is the presence of cloud cover (Lamine et al. 2018). A method that overcomes this problem entirely, and a recent trend in remote sensing for food security and agriculture purposes, is the use of unmanned aerial systems (UAS). Cloud cover becomes no longer an issue due to these instruments operating below the cloud. One such program, a joint collaboration between the Welsh Assembly Government, Environment Systems, and Callen-Lenz Associates is Project URSULA (UAS Remote Sensing for Use in Land Applications). The project explored the potential for advanced remote sensing in land applications, primarily in high-input arable farming (Project URSULA 2013). This furthers research into the farm management strategy known as precision agriculture (PA) (Liaghat and Balasundram 2010). PA aims to bring about an increase in the production efficiency, productivity, and profitability of farms and as such, it contributes to food security as a whole.

EO data collected from Synthetic Aperture Radar (SAR) sensing systems have been used alone in several applications, such as topographic mapping, oceanography, weather forecasting, geology mapping, and crop and forest inventories (Kumar et al. 2016; Mishra et al. 2017; Gupta et al. 2018). The added value of SAR data to LULC mapping has also been demonstrated by several researchers so far. For example, such data has been used to assist improving mapping of forest growth, biomass estimation (Lu et al. 2016), and forest architecture (Lehmann et al. 2015). The benefits of combining optical and SAR datasets to the process of generating a forest inventory and similar products were also recently outlined (De Alban et al. 2018). A forest and non-forest classification with accuracy in excess of 80% was produced (Ling et al. 2012) using multi-temporal alternating polarization (HH, HV) data.

Such data has indeed been shown to be useful in food security applications such as producing agriculture and crop monitoring (Chatziantoniou et al. 2017; Whyte et al. 2018). In terms of the latter, the need for data throughout the growing period has been highlighted and it is noted that when information gaps occur due to haze and/or cloud cover, classification accuracies generally become inadequate (McNairn et al. 2002). The ability of SAR to image throughout day and night while remaining immune to the issue of cloud cover can fill such information gaps during overcast periods and therefore allow for reliable mapping of agricultural crops (Chatziantoniou et al. 2017). For example, Radarsat-2 instrument (C-band instrument) has been used alone in grassland studies and has been shown to provide a good separation of crops and improved grasslands through use of quad-pol (HH, HV, VV, VH) data (Buckley and Smith 2010). Despite this promising potential that the use of SAR data has shown in LULC mapping, to our knowledge, there are very few studies that have explored specifically the use of data from the Envisat ASAR C-Band SAR instrument (Hasager et al. 2015).

In purview of the above, this work aims at exploring the added value of the synergistic use of optical and radar data (from the Landsat TM and ASAR sensors respectively), towards improving the accuracy of land cover classifications from EO datasets. As a case study, the region of Wales in the UK is used. For this area, all the required data was acquired. Such rule-based approaches to classification have been used in the past to guide policy making in Wales. As such, the likelihood of continued use of rule-based classification for future LULC studies in the area is high.

Materials and methods

Study site

The country of Wales lies on the western side of the island of Great Britain and forms part of the UK. It has a coastline of approximately 1400 km and is bordered by England to the east and the Irish Sea to the west; Wales' total land cover is approximately 20,000 km^2 and it is primarily a mountainous country. The study area itself is located in the coastal region of mid-west Wales within Cardigan Bay and has an Ordnance Survey grid reference of SN. Aberystwyth is the main urban area that can be observed in the study area and lies on the mouth of the river Ystwyth to the southwest of the image (Fig. 1). The northern extent is marked by the distinctive Dovey estuary, while eastwards, the study area reaches into the Cambrian Mountains. The total size of the study area is approximately 400 km^2.

Welsh land cover is known for its high diversity (Blackstock et al. 2007). Accordingly, a variety of land cover types are contained within the study area, from the lowlands

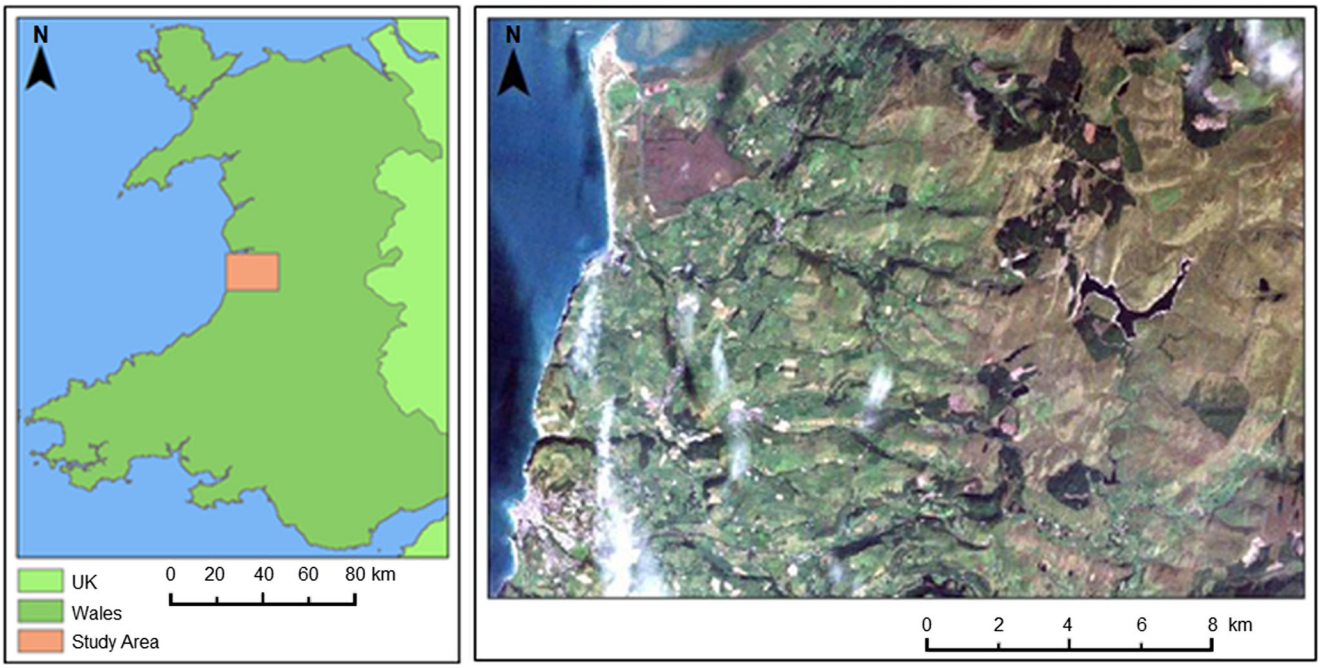

Fig. 1 Location and extent of the study area

near the coast to the uplands in the west of the area. Lowland areas do not exhibit many areas of unimproved grassland and consist mainly of land used for agricultural purposes. Therefore, large amounts of improved grasslands, containing *Lolium perenne*, are present, in addition to arable land. The lowland areas also contain an extensive mass of raised bog located at Borth Bog and, in addition to Aberystwyth, smaller urban settlements are noticeable. The uplands are home to a wide range of ecosystems, which include bogs, heather moors, and water bodies. The most noticeable, in the right-center of the image (Fig. 1), is Nant y Moch reservoir. Furthermore, the Cambrian Mountains account for a large portion of Welsh blanket bog as well as wet and dry heathland. Also found here are areas of Atlantic Oak woodlands (Cambrian Mountains Society 2013). Additional areas of upland woodland consist of Sitka spruce plantations and European larch; broad-leaved and mixed woodlands can be found in the lowlands. Other species found in upland areas include bracken and gorse, in addition to *Vaccinium*- and *Molinia*-dominated marshy grasslands. A substantial amount of dry, wet, and blanket bog with hummock-forming species including *Calluna vulgaris* and *Juncus* are also present. Grasslands include some improved areas, as well as acid and neutral grasslands, and extensive areas of unimproved grassland.

Datasets

Multi-sensor EO datasets were acquired, which included both SAR and optical satellite data. Envisat ASAR Alternating Polarization (AP) was acquired from the Landmap service (http://www.landmap.ac.uk). Data was provided with a Level 0 Alternating Polarization product (AP0) from an ascending orbit. Focusing of the raw data to a Single Look Complex (SLC) image was carried out, followed by multi-looking to improve the radiometric resolution of the data at the expense of the spatial resolution. This is achieved by processing portions of the signal responses individually before combining them to create the final result of an *N*-look image, where *N* is the number of processed portions, or looks (Rees 1999). A spatial resolution of 25 m was achieved. As a result of the multi-looking process, speckle is reduced. However, for further speckle reduction, an additional spatial filter was applied utilizing a moving window across the image. Landmap used the Frost filter, described as an adaptive filter, which calculates the pixel values within a window using an adaptive exponential impulse response (Sarmap 2007). A 5 × 5 pixel window size was used.

The images were then geocoded and terrains corrected using 75 m Shuttle Radar Topographic Mission (SRTM) data and were projected to the British National Grid. Lastly, radiometric calibration was carried out to produce image data displaying the geocoded backscattering coefficient (Sigma-nought, σ^0) values as a linear (decimal) figure. The backscattering coefficient is a conventional measure of the strength of radar signals reflected by a distributed scatterer. Therefore, it denotes the effectiveness of a surface at scattering the radiation incident upon it (Rees 1999). The steps detailed above were carried out using the SARscape extension in ENVI 5.0. The end-result, and thus the dataset provided by Landmap, consists of two coherent grayscale SAR images (HH and HV) in GeoTiff format. The images are projected to the British National Grid at 25 m spatial resolution with pixel values to correspond to the backscattering coefficient.

In addition to the above data, optical imagery from Landsat 5 TM sensor was acquired from the USGS GloVis service (available at http://glovis.usgs.gov). Landsat 5 had a repeat cycle of 16 days and carried a MSS instrument along with the TM (Loveland and Dwyer 2012). A Level 1T product was downloaded, meaning that it had already been geometrically corrected and orthorectified using ground control points from the Global Land Survey 2000 (GLS2000). The data was acquired as a GeoTiff file in raw digital number format. The location of the full scene acquired was at Path 204, Row 23, as close as possible to that of the SAR data. No significant cloud cover was present in the total scene (field of view coverage of 170 km × 185 km). The data was provided resampled to the Universal Transverse Mercator (UTM) Zone 30N—World Geodetic System (WGS) 84 geographic projection using the cubic convolution method (United States Geological Survey 2013). Overall, spatial resolution was 30 m in the reflectance bands and 60 m in the thermal band.

In a shapefile containing the administrative boundaries of Wales was acquired and used in the validation of data georeferencing. The file was provided by DIVA-GIS,[1] a free web-based spatial data resource. Additionally, a digital elevation model (DEM) for the study area was acquired at a 30 m spatial resolution to be used as a factor in the classification process. A further supplementary dataset, the Phase 1 habitat map, was acquired in shapefile format and used as a reference when selecting appropriate representative training areas. It should be noted that the Phase 1 habitat map dates back to the year 1997, and therefore, land cover may have changed between the completion of the map and the acquisition of the satellite data. As such, it was used as a guide only, with thought given to land cover observed in the Landsat scene, reference to high-resolution imagery available through Google Earth, as well as personal knowledge of the area developed through a field study. The Phase 1 habitat map was acquired through the Countryside Council for Wales's website (available at http://www.ccw.gov.uk/landscape%2D%2Dwildlife/habitats-species/terrestrial/habitats/habitat-surveys.aspx?lang=en). A summary of all the satellite data used in this study is provided in Table 1.

Table 1 Satellite data acquired and their key specifications

	Optical dataset	SAR dataset
Sensor name	Landsat 5 TM	Envisat ASAR
Date of acquisition	Sept. 13, 2003	Sept. 25, 2003
Spatial resolution	30 m	25 m
Band information	Blue (0.45–0.52 μm) Green (0.52–0.60 μm) Red (0.63–0.69 μm) NIR (0.76–0.90 μm) MIR (1.55–1.75 μm) TIR (10.40–12.50 μm) MIR (2.08–2.35 μm)	C-Band (5.6 cm)
Polarization		HH/HV

Pre-processing

The first pre-processing step consisted of the radiometric correction of the Landsat TM data to Top of Atmosphere (TOA) reflectance. Additionally, the ASAR AP intensity product was converted to the backscatter coefficient in units of decibels (dB; Whyte et al. 2018). Georeferencing and subsetting of the data then followed, after which a cloud and cloud shadow mask was generated. Next, followed the derivation of further data products in the form of radar texture measures and the Normalized Difference Vegetation Index (NDVI), as well as the generation of a synergistic data file, which is used in the sample selection, rule set generation, and classification processes. The process of TOA correction was subsequently carried out to convert the digital numbers (DNs) in the raw data to meaningful reflectance values suitable for interpretation. The USGS provided the data as separate image bands in GeoTiff format. Band calibration was therefore carried out individually using the Landsat Calibration tool in ENVI before being combined into a single GeoTiff file. This study made use of the reflectance bands only (i.e., bands 1–5 and 7). Georeferencing is the process of spatially aligning datasets to ensure that they are aligned to the same geographical area. The importance of it as a pre-processing step must be stressed when working with data from different sensors and at different spatial resolutions (Petropoulos et al. 2012a). The shapefile representing the boundary of Wales was used to validate the projection. Additionally, the DEM was acquired at this projection and the alignment validated similarly. Due to its geometric accuracy, the Landsat TM scene was chosen to act as a base image onto which the ASAR AP (distorted image) data would be warped. A sub-pixel registration accuracy (i.e., accuracy in a level smaller than the area covered by a pixel) was obtained, which was deemed satisfactory (Petropoulos et al. 2013). Finally, the areas of cloud and cloud shadow within the imagery were removed using a mask produced by manually digitizing the areas covered by clouds. Thus, thematic layers were created allowing these areas to be classified and therefore masked from the rule-based classification process (Clerici et al. 2017).

Derived products

Texture measures were computed for both the HH and HV polarized ASAR images, similarly to other relevant studies (e.g., Laurin et al. 2013). Radar data generally exhibits a high amount of texture in comparison to optical data due to the

[1] www.diva-gis.org

complex interactions of the radar signal (Haack et al. 2000). Texture data can therefore better classify areas where there is not necessarily a unique reflectance or backscatter value, but a variance of the value. The incorporation of various forms of digital texture measurements has been shown to improve classification accuracies (Singh et al. 2016; Chatziantoniou et al. 2017; Whyte et al. 2018). The methods used herein to extract the texture measures were based on the use of the gray level co-occurrence matrix (GCLM). This matrix is used as a foundation on which textural variation can be quantified (Sonka et al. 1998). These measures are calculated using moving array of cells referred to as a window. The texture value of the center cell within the window is derived through a mathematical equation which considers all cell values within the moving window (Haralick et al. 1973).

The NDVI was used for acquiring the phenological information regarding the land cover represented within each image. NDVI values were estimated on a per-pixel basis using the corresponding bands of the TM instrument (band 3 represents the red reflectance values and band 4 the NIR reflectance values). In addition to the generation of the NDVI and SAR texture products, the data was merged to form a single multiband GeoTiff file: the synergistic dataset. This consisted of the six reflective bands of the TM instrument assigned to bands 1 through 6, with bands 7 and 8 corresponding to the ASAR backscatter coefficient values in decibels at HH and HV polarizations, respectively. The NDVI was assigned to band 9 and the following five bands, from 10 to 14, contained the texture measures. In order, these were the mean, variance, homogeneity, entropy, and correlation texture data calculated from the HH polarized ASAR image using a 9×9 window size. The same texture measures corresponding to the HV polarized image make up bands 15 through 19. The final ten bands (20 through 29) are comprised of the same HH and HV texture measures, calculated using a 13×13 moving window. In addition to providing a container for the data, the synergistic data file allowed the incorporation of the SAR data and texture measures in the generation of color composite images. The latter allowed for a better visual interpretation of the study area.

Classification

The approach adopted to produce the two thematic maps, one based on the optical data and the other produced using the synergistic dataset, was based on an object-based image analysis (OBIA) approach. The analysis of EO data using OBIA has seen increased attention within the past decade (Whyte et al. 2018). It differs from the more traditional pixel-based approach by analyzing groups of pixels together as opposed to each pixel individually. In this study, all analysis was carried out in Trimble eCognition Developer (Trimble 2013), a commercial OBIA software package. Implementation of OBIA for image classification consists of a segmentation process followed by a classification of the segments into user-specified classes. Here, image segmentation was performed using the multi-resolution segmentation algorithm. This bottom-up region-merging technique uses an algorithm which considers each pixel as a separate object before merging similar pixels to form larger image objects, or segments (Rahman and Saha 2008). Pixels are only merged to form segments when a segment homogeneity criterion is satisfied. This criterion is determined through definition of scale, shape, and compactness parameters, which specify the properties that the resulting segments should have (Aguilar et al. 2016).

An initial chessboard segmentation using a scale parameter of 1 was executed, resulting in each pixel becoming a separate segment. This allowed individual pixels displaying areas of cloud and cloud shadow to be classified as such, and thus, only the cloud-free image data to be segmented for the rule-based classification. The remaining unclassified pixels were classified as either uplands or lowlands based on thresholding the DEM. Areas below an elevation of 260 m were classified as lowlands and those above this height classified as uplands. Subsequently, these areas were individually segmented to appropriate sized segments through use of the multi-resolution segmentation algorithm.

Having masked out cloud and cloud shadow and established appropriately sized image segments, the next step was to select sample areas for the classes. As this study is interested in demonstrating the added value of SAR data to the classification process, certain control measures were implemented. The first of these was the use of a common set of sample areas. This was to ensure that any greater separability that may arise from one approach would not be the result of better sample area selection. Similarly, the second control measure was to ensure that the accuracy assessment of both thematic maps would make use of the same set of test areas. This was necessary to allow a comparison of the accuracy of each classification.

The chosen classes were the generalized land use/cover types that can be observed in the study area: improved grasslands, unimproved grasslands, arable/dry land, raised bog, urban, woodlands, standing water, and sea. Sample areas were selected for each of these classes based on a combination of visualizing different color composites of the data, using personal knowledge and the examination of the Phase 1 map in addition to higher resolution satellite imagery (from Google Earth). The samples per class are shown in Tables 2 and 3 and they are as follows: standing water 9, woodland 18, improved grasslands 9, raised bog 5, sea 4, urban 11, arable/dry land 6. Naturally, visual examination and experience of interpreting satellite imagery was sufficient for the selection of sea, standing water, and urban sample areas. The addition of study area knowledge allowed for the selection of areas of raised bog. In addition to the previous selection methods, improved grasslands, unimproved grasslands, woodland, and arable/dry land

Table 2 Confusion matrix corresponding to the LULC map produced by the optical approach (Fig. 3). *UP* uplands, *LOW* lowlands, *SW* standing water, *W* woodland, *IG* improved grasslands, *UG* unimproved grasslands, *RB* raised bog, *S* sea, *U* urban, *A/D* arable/dry land. Italicized entries indicate correct allocations

	Sample										
Classification	UP	LOW	SW	W	IG	UG	RB	S	U	A/D	Sum
UP	*0*	0	4	4	0	1	0	0	0	0	9
LOW	0	*0*	0	2	0	0	2	0	2	0	7
SW	0	0	*5*	0	0	0	0	0	0	0	5
W	0	0	0	*11*	0	0	0	0	0	0	10
IG	0	0	0	0	*13*	2	0	0	0	0	15
UG	0	0	0	0	1	*6*	0	0	2	0	9
RB	0	0	0	0	0	0	*3*	0	0	0	3
SW	0	0	0	0	0	0	0	*4*	0	0	4
U	0	0	0	0	0	0	0	0	*6*	2	8
A/D	0	0	0	0	0	0	0	0	1	*4*	5
Sum	0	0	9	17	14	9	5	4	11	6	75
Overall accuracy	0.69								Total correct		52
Kappa coefficient	0.65										

areas were selected by further referring to the Phase 1 map overlaid onto the Landsat TM data. High-resolution satellite imagery available from Google Earth was examined over these areas to provide some validation. Only areas which had shown no extensive temporal change were chosen as samples. The mean spectral responses from the samples for each class are provided in Fig. 2.

The selection of class sample areas allowed for the examination of their corresponding reflectance, backscatter, elevation, texture, and NDVI characteristics. It was with this information that rule sets with the goal of classifying the land cover into the given classes were generated. Two separate rule sets and classifications were produced. The first was generated through consideration of class responses in the Landsat TM bands, NDVI, and the DEM of the study area. The second rule set considered these in addition to incorporating the ASAR HH and HV backscatter coefficients, as well as the corresponding texture measures and the difference and ratio images. In both cases, the feature histograms for each class were examined extensively to determine those features which allowed for a greater degree of separation between the classes. Rules were then developed to act as conditions that a segment must satisfy in order to be classified as the respective class. Single thresholds were used in addition to simple Boolean operations and more complex fuzzy membership functions. Following the application of each rule set

Table 3 Confusion matrix corresponding to the LULC map produced by the synergistic approach (Fig. 4). Notation is explained in Table 2. Italicized entries indicate correct allocations

	Sample										
Classification	UP	LOW	SW	W	IG	UG	RB	S	U	A/D	Sum
UP	*0*	0	3	0	0	1	0	0	0	0	4
LOW	0	*0*	0	0	0	0	0	0	2	2	4
SW	0	0	*6*	0	0	0	0	0	0	0	6
W	0	0	0	*17*	0	0	0	0	0	0	17
IG	0	0	0	0	*13*	2	0	0	0	0	15
UG	0	0	0	0	1	*6*	0	0	1	0	8
RB	0	0	0	0	0	0	*5*	0	0	0	5
SW	0	0	0	0	0	0	0	*4*	0	0	4
U	0	0	0	0	0	0	0	0	*8*	0	8
A/D	0	0	0	0	0	0	0	0	0	*4*	4
Sum	0	0	9	17	14	9	5	4	11	6	75
Overall accuracy	0.84								Total correct		63
Kappa coefficient	0.81										

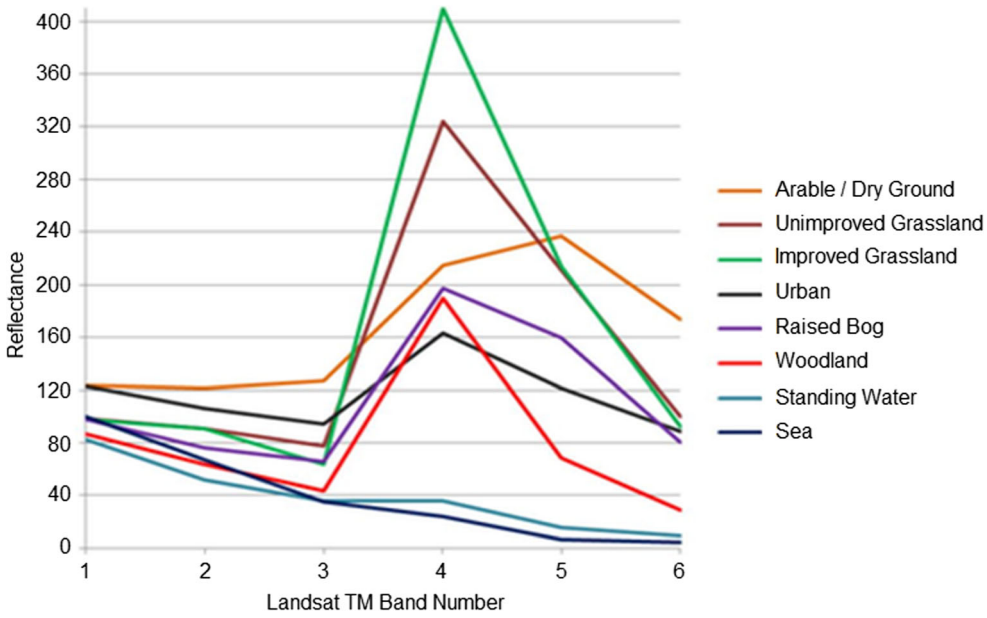

Fig. 2 Spectral response of each class across the Landsat TM bands (band 6 on the graph corresponds to band 7 of the TM instrument (SWIR2))

to the image data, a corresponding thematic map was produced. To aid visual interpretation, all segments within a class were merged into larger image objects. The results of both classification procedures were subsequently exported as shapefiles, with attribute tables containing the class names, for further manipulation.

Results

As a result of the individual classifications of the optical and synergistic approaches, two corresponding thematic maps of LULC were produced, which are presented below together with the accuracy assessment results.

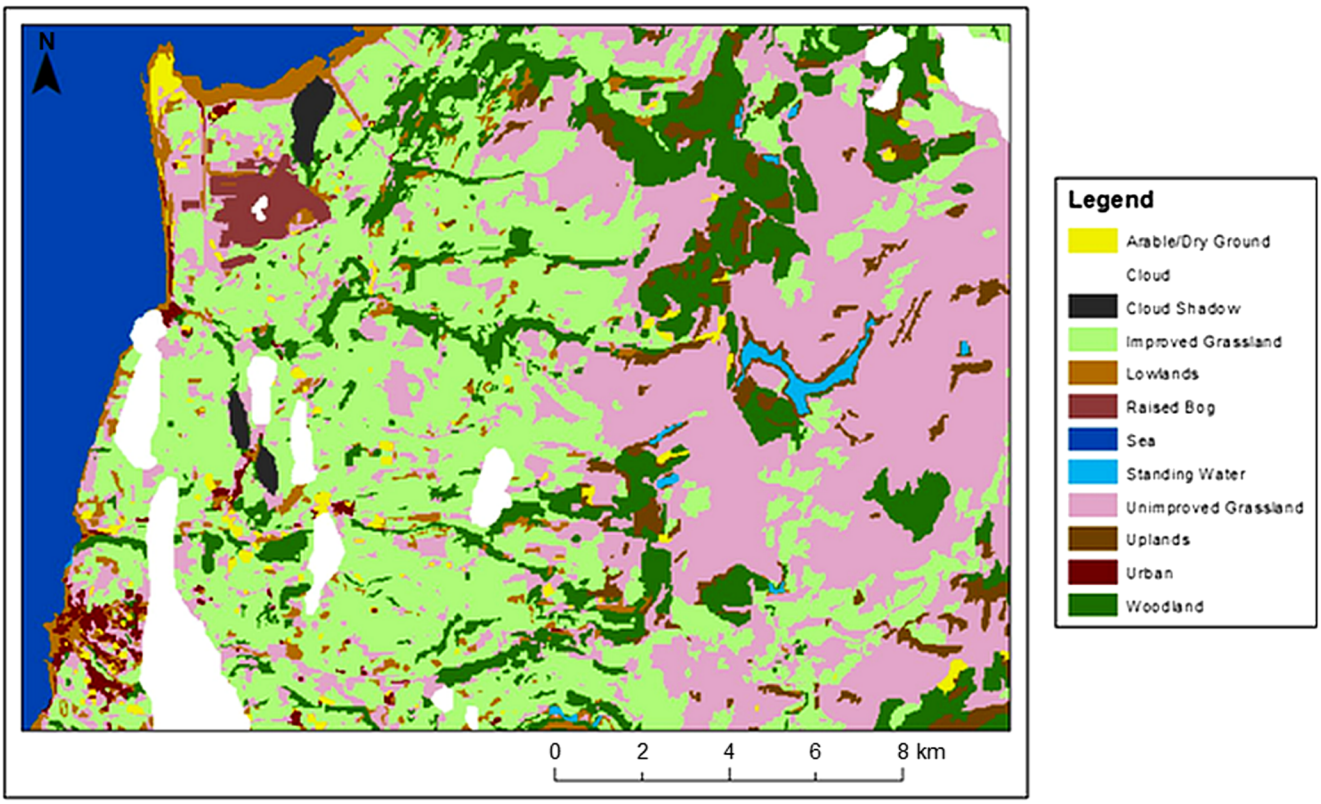

Fig. 3 LULC thematic map produced using the optical classification approach

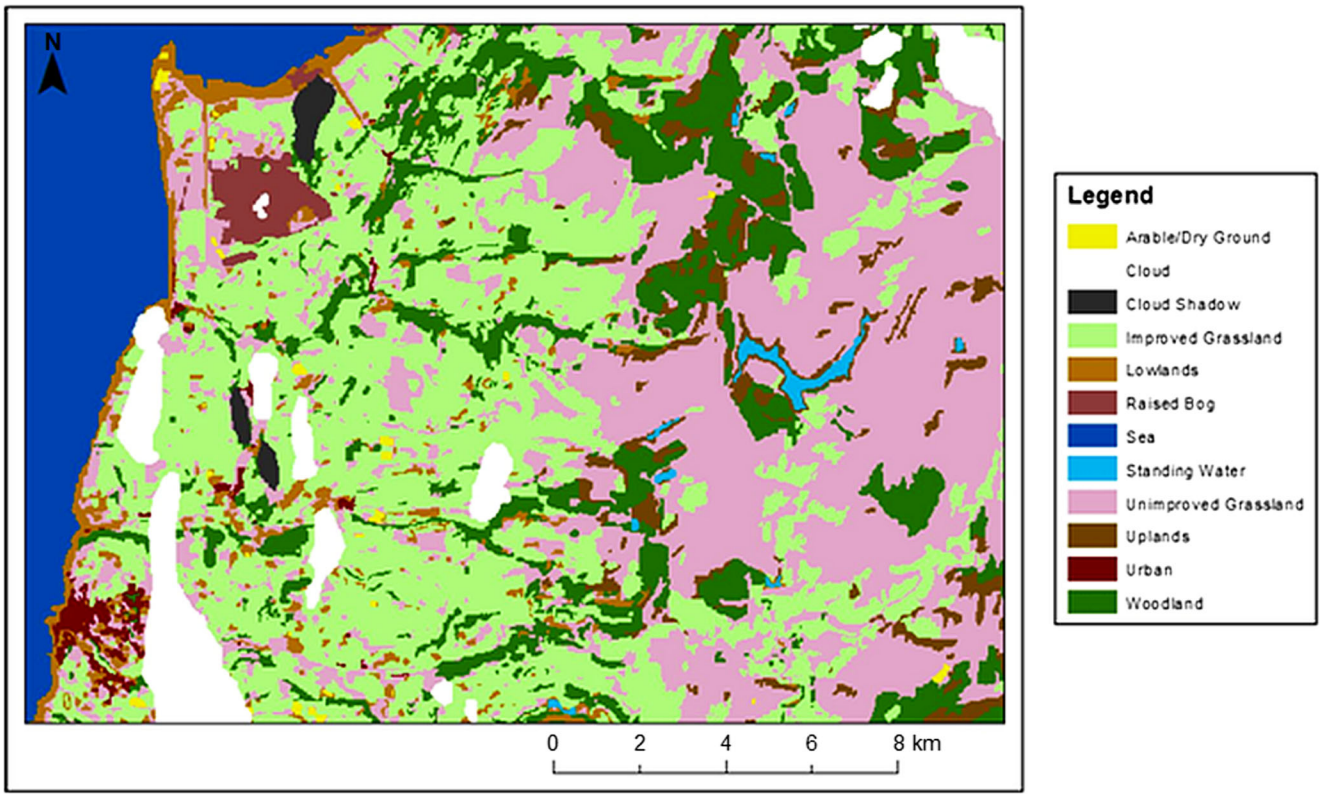

Fig. 4 LULC thematic map produced using the synergistic (i.e., optical and RADAR) classification approach

LULC classifications

The resulting thematic maps based on the optical and synergistic approaches are shown in Figs. 3 and 4, respectively. Firstly, sea was separable from the other classes through a characteristically low NDVI as well as SWIR values. Using the synergistic approach, the backscatter values for HH in decibels allowed for a higher degree of separability of the sea class. This was due to the prevalence of surface reflectance, and therefore, the HH dB feature was used in this rule set. The thresholds used to classify the standing water class in the optical approach were also based on the NDVI and SWIR1 features, with the inclusion of blue reflectance to separate it from the similar sea class. In the rule set generated for the synergistic approach, the backscatter values observed at the HV polarization were very distinguishing features of standing water. Due to the stationary nature of water bodies such as lakes, surface scattering is high. Conversely, very little volumetric scattering takes place and as a result, the backscatter measured at the HV setup was very low. Furthermore, it was consistently low over the sample areas and as such, the main feature selected for this class was the mean texture measure derived from the HV polarized image. It appeared that the window sizes used in the generation of the texture measures, in this case and overall, did not have a large effect on the observed separability of the classes; any differences were negligible.

Urban areas and areas of arable/dry land were quite similar spectrally. Even with the use of the NDVI and DEM, there was some overlap between the classes. However, these two classes became immediately separable on examination of the SAR data, both at the HH and HV polarizations. This is attributed to the different scattering/reflectance mechanisms observed; arable land is generally flat land, meaning surface reflectance is more prominent. A much greater degree of volumetric scattering was observed in the urban class when compared to arable/dry land and the neighboring classes in the image. Furthermore, the HV correlation texture measure was able to highlight this fact and as a result, both the HV dB and the HV correlation (using a 9 by 9 window) features were used in the synergistic classification of urban areas.

Arable/dry land areas on the other hand were classified using the mean, variance, and homogeneity texture measures derived from the HH polarization. This was because not only did these areas show greater surface scattering, but there was little variance in this, and the backscatter values were largely consistent over the areas. Again, the textures produced using a 9 by 9 window were used.

Another class which was shown to be highly separable in the SAR data was woodland. In the optical classification approach, the NDVI and SWIR2 reflectance values were used in the rule set, as well as reflectance in the green band. With the incorporation of the SAR data, it was clear to see the

woodland areas due to the large amount of volume scattering that is characteristic of such areas. Therefore, the backscatter values at HV polarization were used in the synergistic rule set in place of the reflectance in the green band. The result was that the synergistic classification (Fig. 4) was able to pick up more of the smaller areas of woodland in the study area, including some areas near the Dinas Reservoir (found in the lower right corner of the map), as well as small areas in the lowlands.

Borth Bog, the prominent region of raised bog in the study area, was classified in the optical approach through use of the NDVI as well as the DEM, as it exists at a very low elevation. In addition, its reflectance at the green and SWIR1 bands were selected as they were shown to be quite definitive. When examining Borth Bog in the SAR imagery, the samples showed a largely consistent value of backscatter at the HH polarization. This was highlighted in the HH variance texture measure (9 by 9 window size) and was therefore used in the synergistic rule set along with the NDVI and DEM thresholds. When examining the two classifications, the synergistic result has classified a larger area of raised bog.

The final two classes of improved and unimproved grasslands were shown to be spectrally similar; Fig. 2 illustrates this point well. As a result, the optical-based rule set of the two classes was built around the NDVI and the reflectance in the red and NIR bands. Improved grasslands, generally being healthier, exhibited a characteristically higher NDVI value than the unimproved grasslands and therefore a simple threshold was applied. However, the reflectance of the two classes in the red and NIR bands varied. As a result, fuzzy membership functions were computed and used in the rule set for each class.

Notably, the incorporation of the SAR data did not enhance the separability of these classes. After thorough examination of the backscatter responses and texture measures, it was apparent that no SAR-derived feature would further aid the classification. The features which mostly defined these two classes remained to be the NDVI and the red and NIR reflectance values. This illustrates that, in this case, the difference between the two classes came down to their spectral properties as opposed to their structural properties.

Accuracy assessment and McNemar's test

The final steps consisted of performing an evaluation of classification accuracy followed by a direct comparison using McNemar's test (Foody 2004). This is a parametric, very simple to understand and execute statistical test that can be used in evaluating the superiority of one thematic map over another using the same validation sample, as was the case in the present study. The test is based upon the standardized normal test chi-square (χ^2) statistic computed from a two by two matrix based on correctly and incorrectly classified pixels in both classifications using Eq. 1 (Foody 2004; De Leeuw et al. 2006):

$$\chi^2 = (f_{12} - f_{21})^2 / (f_{12} + f_{21}) \quad , \tag{1}$$

where f_{12} denotes the number of cases that are correctly classified by classifier one but incorrectly classified by the classifier two, and f_{21} denotes the number of cases that are correctly classified by classifier two but wrongly classified by the classifier one (Manandhar et al. 2009; Petropoulos et al. 2012a, b). Thus, this test is focused on the binary distinction between correct and incorrect class allocations that are derived directly from the comparison of the error matrices between the two classifications compared. The derived χ^2 value from the implementation of this test is subsequently compared versus tabulated χ^2 values to indicate its statistical significance of the differences between the compared thematic map products. The McNemar test was implemented herein two times, comparing the classification maps derived between the two scenarios (optical data only and optical plus SAR), for each classification technique applied. In our study, χ^2 values were compared for the 95% level of confidence respectively.

The confusion matrices corresponding to the optical and the synergistic classification approaches are shown in Tables 2 and 3, respectively. Table 4 provides the contingency table, forming the basis of McNemar's test. When compared to the critical value for the 95% confidence interval (3.84), the chi-squared value calculated above is greater than the critical value. Thus, the condition on which to reject the null hypothesis is satisfied and the alternative hypothesis is accepted. Therefore, McNemar's test clearly shows a significant improvement in the LULC classification produced through the synergistic approach over that produced through the optical approach. Furthermore, the chi-squared value of 11 is greater than the critical value of even the 99.9% confidence interval (10.83). Therefore, not only is the improvement in the classification result statistically significant at the 95% confidence interval, but it is significant up to the 99.9% confidence interval.

Discussion

The incorporation of the SAR data and derived texture measures increased classification accuracy. However, the accuracy of the optical classification approach alone is surprisingly low considering the basic land covers used. This can be largely attributed to the test area distribution, as over one-third of the test areas were in the woodland and urban classes. Notably, those classes were more accurately determined through the synergistic approach. However, it can be seen from the confusion matrices and from visual comparison of the two thematic maps that the synergistic approach did perform better in overall, and the improvement in accuracy was statistically

significant. Therefore, these results put forward a strong case for further development of the methods shown here to provide more research into synergistic LULC classifications.

The inability of the SAR data to provide separation of the improved and unimproved grasslands observed in this study is attributed to the wavelength of the Envisat ASAR instrument relative to the scattering features of these classes; from the C-band perspective, both classes appeared to exhibit a similar surface roughness. The wavelength of the ASAR instrument is approximately 5.6 cm; therefore, due to the similarity observed in the class responses, it can be inferred that overall the classes were shown to have scattering objects of a similar size and distribution. It is therefore understood that the use of X-band SAR data over the study area would aid in the separation of these classes due to its use of a smaller wavelength (3 cm). Furthermore, the TerraSAR-X instrument can provide quadrature-polarized (quad-pol) data (HH, VV, HV, VH), with which polarimetry can be further investigated. Buckley and Smith (2010) demonstrated the benefits associated with the quad-pol setup.

In respect to the texture measures used in this study, derived from the ASAR data, there were negligible differences observed between those generated using a 9 by 9 window and those generated using a 13 by 13 window. This can be attributed to the fact that some of the land cover types manifest on a large scale, and therefore, in general, the 9 by 9 and 13 by 13 pixel windows pick up a similar distribution of data values. For large-scale applications, window sizes of 15 by 15, 31 by 31, and 61 by 61 have been shown to provide constructive results (Blom and Daily 1982).

In regard to the rule-based classification method that was used in this study, the image classification strategy implemented here made use of a rule-based procedure as implemented by Haack et al. (2000). Several other studies in Wales, concerned with producing land cover classifications either on a relatively small scale (Lucas et al. 2007) or country-wide scale (Lucas et al. 2011), have also diverged from the semi-automated approach. This procedure has been used over the study area previously and has been shown to be a reliable method of classification (Lucas et al. 2011). This method allows prior knowledge to be incorporated and the integration of additional data as it becomes available. Therefore, the likelihood of the rule-based approach being used for future LULC in Wales is high. As such, in this study's aim to demonstrate the added value of SAR data in a LULC classification in Wales, it was appropriate to implement a rule-based classification approach.

Therefore, the methodology implemented herein is one that is capable of being applied across Wales or even the UK and has the ability to adapt to the generation of more information. Further development and improvement of the results could arise from several approaches. Firstly, the use of multi-temporal data could allow for the inclusion of rules based on land cover phenology and morphology. The integration of shorter wavelength SAR data—the use of X-bad SAR data, such as that provided by the TerraSAR-X instrument, could facilitate further discrimination between improved and unimproved grassland areas. Furthermore, a quad-pol setup could allow for a deeper investigation into SAR polarimetry. Besides, the use of fractional images, derived from optical data, has been shown to be of benefit to LULC classifications (Lu and Weng 2004). Such images show the relative proportions of different components (or endmembers) that make up a pixel. Finally, the use of EO data with a finer spatial resolution would enhance the spatial separability of the classes.

Table 4 Contingency table based on confusion matrices shown in Tables 2 and 3

	Synergistic approach		
Optical approach	Correct	Incorrect	Total
Correct	52	0	52
Incorrect	11	12	23
Total	63	12	75

Conclusions

In the present study, Landsat TM data was used alone as a basis for producing a LULC map of an area of Wales. In addition, a methodology was developed to allow the incorporation of Envisat ASAR data and derived texture measures into the process, thus developing a synergistic LULC classification approach. The two approaches were evaluated using the traditional method of the comparison of the overall accuracies.

This evaluation was then expanded by a statistical assessment of the results; a hypothesis-based testing framework was implemented through the use of McNemar's test. The results show that not only was the synergistic classification of a greater accuracy (improvement from 69 to 84%), but the improvement was shown to be statistically significant at the 99.9% confidence level. Therefore, this study has demonstrated the potential benefits of a synergistic approach to LULC. The methodology implemented in this study has the ability to adapt to more data or more recent data, after the necessary adjustment take place (e.g., in regard to preprocessing steps that needed to be implemented). With continued contributions of free data from Landsat, the proposed methodology has the potential to provide significant improvement in precision agriculture and land use policies. The possible inclusion of survey data gathered from unmanned aerial vehicles (drones) are expected to contribute to more accurate classification.

With the availability of data from the Sentinel missions, a greater amount of EO data is already available from different

sensor types and resolutions. The ability to refine the classification with more up-to-date, reliable data is important when the data is used to inform food security policy makers—whether they are responsible for global or European polices, or smaller-scale issues. Furthermore, as Sentinel data is free of charge, it is possible to produce reliable and timely LULC maps for food security purposes at relatively low costs overall. This is especially important when considering smaller-scale food security projects such as those in the field of precision agriculture (PA). PA investigations usually take place on a small scale and the work can include land management studies, crop mapping/monitoring, and field surveys to monitor disease. All of the information gathered this way can feed into larger scale food security models and policy decisions. Therefore, it is important that such investigations continue to take place in the future. This remains to be seen.

Acknowledgments Authors are grateful to the reviewers for their comments that resulted to improving the overall manuscript. GPP's contribution to this work has been supported by the EU Marie Curie Project ENViSIon-EO (project contract ID 752094).

Author contributions AC conducted the research described in this study under the supervision and guidance of GPP, and all co-authors contributed to the preparation of this manuscript for submission to the journal and also during the paper revision.

References

Aguilar MA, Aguilar FJ, Lorca AG, Betlej GM, Cichon P, Nemmaouni A, Vallario A, Parente C (2016) Assessment of multi-resolution segmentation for extracting greenhouses from Worldview-2 imagery. Int Arch Photogramm Remote Sens Spat Inf Sci XLI-B7 2016, XXIII ISPRS Congress, 12–19 July 2016, Prague, Czech Republic

Bao Y, Lin L, Wu S, Deng KAK, Petropoulos GP (2018) Surface soil moisture retrievals over partially vegetated areas from the synergy of Sentinel-1 & Landsat 8 data using a modified water-cloud model. Int J Appl Earth Obs Geoinf 72:76–85

Blackstock TH, Burrows CR, Howe EA, Stevens DP, Stevens JP (2007) Habitat inventory at a regional scale: a comparison of estimates of terrestrial Broad Habitat cover from stratified sample field survey and full census field survey for Wales, UK. J Environ Manag 85(1):224–231

Blom RG, Daily M (1982) Radar image processing for rock-type discrimination. IEEE Trans Geosci Remote Sens 20(3):343–351

Buckley JR, Smith AM (2010) Monitoring grasslands with radarsat 2 quad-pol imagery. Honolulu, Hawaii, 2010. Geoscience and Remote Sensing Symposium

Cambrian Mountains Society (2013) Cambrian Mountains society-biodiversity-landscape. [Online] Available at: http://www.cambrian-mountains.co.uk/landscape- biodiversity.php [Accessed May 2018]

Chatziantoniou A, Petropoulos GP, Psomiadis E (2017) Co-orbital Sentinel 1 and 2 for LULC mapping with emphasis on wetlands in a Mediterranean setting based on machine learning. Remote Sensing MDPI 9:1–878. https://doi.org/10.1080/10106049.2017.1307460

Clerici N, Valbuena Calderón CA, Posada J (2017) Fusion of Sentinel-1A and Sentinel-2A data for land cover mapping: a case study in the lower Magdalena region, Colombia. J Maps 13(2):718–726. https://doi.org/10.1080/17445647.2017.1372316

De Alban JDT, Connette GM, Oswald P, Webb EL (2018) Combined Landsat and L-band SAR data improves land cover classification and change detection in dynamic tropical landscapes. Remote Sens 10(2):306. https://doi.org/10.3390/rs10020306

De Leeuw J, Jia H, Yang L, Liu X, Schmidt K, Skidmore AK (2006) Comparing accuracy assessments to infer superiority of image classification methods. Int J Remote Sens 27:223–232

Elatawneh A, Kalaitzidis C, Petropoulos GP, Schneider T (2012) Evaluation of diverse classification approaches for land use/cover mapping in a Mediterranean region utilizing Hyperion data. Int J Digital Earth 7:1–23. https://doi.org/10.1080/17538947.2012.671378

European Space Agency (2013) Contributing Missions overview / Copernicus / Observing the Earth / Our Activities / ESA. [Online] Available at: http://www.esa.int/Our_Activities/Observing_the_Earth/Copernicus/Contributing_Missions_overview [Accessed Augustus 2013]

Food and Agriculture Organization of the United Nations (2012) The state of food insecurity in the world. Food and Agricultural Organisation of the United Nations

Foody GM (2004) Thematic map comparison: evaluating the statistical significance of differences in classification accuracy. Photogramm Eng Remote Sens 70(5):763–767

Gómez C, White JC, Wulder MA (2016) Optical remotely sensed time series data for land cover classification: a review. ISPRS J Photogramm Remote Sens 116:55–72. https://doi.org/10.1016/j.isprsjprs.2016.03.008

Gupta DK, Prasad R, Kumar P, Srivastava PK, Islam T (2018) Robust machine learning techniques for rice crop variables estimation using multiangular bistatic scattering coefficients. J Appl Remote Sens 12(03):1

Haack BN, Herold ND, Bechdol MA (2000) Radar and optical data integration for land-use/land-cover mapping. Photogramm Eng Remote Sens 66(6):709–716

Haralick RM, Shanmugan K, Dinstein I (1973) Textural features for image classification. IEEE Trans Syst Man Cybern 3(6):610–621

Hasager CB, Mouche A, Badger M, Bingöl F, Karagali I, Driesenaar T, Stoffelen A, Peña A, Longépé N (2015) Offshore wind climatology based on synergetic use of Envisat ASAR, ASCAT and QuikSCAT. Remote Sens Environ 156:247–263

Joint Research Centre (2013) About us / MARS Unit - MARS. [Online] Available at: http://mars.jrc.ec.europa.eu/mars/About-us [Accessed Augustus 2013]

Kumar P, Prasad R, Choudhary A, Narayan Mishra V, Kumar Gupta D, Srivastava PK (2016) A statistical significance of differences in classification accuracy of crop types using different classification algorithms. Geocarto Int 1–34

Lamine, S. G.P. Petropoulos, S.K. Singh, s. Szabo, N Bachari, P.K. srivastava & S. Suman (2018): Quantifying land use/land cover spatio-temporal landscape pattern dynamics from Hyperion using SVMs classifier and FRAGSTATS. Geocarto Int, in press, https://doi.org/10.1080/10106049.2017.1307460, 33, 862, 878

Laurin GV et al (2013) Optical and SAR sensor synergies for forest and land cover mapping in a tropical site in West Africa. Int J Appl Earth Obs Geoinf 21:7–17

Lehmann EA, Caccetta P, Lowell K, Mitchell A, Zhou ZS, Held A, Milne T, Tapley I (2015) SAR and optical remote sensing: assessment of complementarity and interoperability in the context of a large-scale operational forest monitoring system. Remote Sens Environ 156:335–348. https://doi.org/10.1016/j.rse.2014.09.034

Liaghat S, Balasundram SK (2010) A review: the role of remote sensing in precision agriculture. Am J Agric Biol Sci 5:50–55

Ling F et al (2012) Forest and non-Forest mapping with Envisat ASAR images. Journal of Remote Sensing (China) 16(5):1101–1114

Loveland TR, Dwyer JL (2012) Landsat: building a strong future. Remote Sens Environ 122:22–29

Lu D, Weng Q (2004) Spectral mixture analysis of the urban landscape in Indianapolis with Landsat ETM+ imagery. Photogramm Eng Remote Sens 70(9):1053–1062

Lu D, Chen Q, Wang G, Liu L, Li G, Moran E (2016) A survey of remote sensing-based aboveground biomass estimation methods in forest ecosystems. International Journal of Digital Earth 9(1):63–105. https://doi.org/10.1080/17538947.2014.990526

Lucas R, Rowlands A, Brown A, Keyworth S, Bunting P (2007) Rule-based classification of multi-temporal satellite imagery for habitat and agricultural land cover mapping. ISPRS Journal of Photogrammetry & Remote Sensing 62(3):165–185

Lucas R, Medcalf K, Brown A, Bunting P, Breyer J, Clewley D, Keyworth S, Blackmore P (2011) Updating the Phase 1 habitat map of Wales, UK, using satellite sensor data. ISPRS Journal of Photogrammetry & Remote Sensing 66:81–102

Manandhar R, Odeh Inakwu OA, Ancev T (2009) Improving the accuracy of land use and land cover classification of Landsat data using post-classification enhancement. Remote Sens 1(3):330–344

McNairn H, Ellis J, van der Sanden JJ, Hirose T, Brown RJ (2002) Providing crop information using RADARSAT-1 and satellite optical imagery. Int J Remote Sens 23(5):851–870

Mishra VN, Prasad R, Kumar P, Gupta DK, Srivastava PK (2017) Dual-polarimetric C-band SAR data for land use/land cover classification by incorporating textural information. Environ Earth Sci 76:26

Petropoulos GP, Kalaitzidis C, Vadrevu KP (2012a) Support vector machines and object-based classification for obtaining land use/cover cartography from Hyperion hyperspectral imagery. Comput Geosci 41:99–107. https://doi.org/10.1016/j.cageo.2011.08.019

Petropoulos, G.P., C. C. Kontoes &. I. Keramitsoglou (2012b): Land cover mapping with emphasis to burnt area delineation using co-orbital ALI and Landsat TM imagery. Int J Appl Earth Obs Geoinf, 18, 344–355, DOI https://doi.org/10.1016/j.jag.2012.02.004

Petropoulos GP, Partsinevelos P, Mitraka Z (2013) Change detection of surface mining activity and reclamation based on a machine learning approach of multi-temporal Landsat TM imagery. Geocarto Int:1–20. https://doi.org/10.1080/10106049.2012.70664

Project URSULA (2013) About. [Online] Available at: http://www.projectursula.com/?page_id=2 [Accessed Augustus 2013]

Rahman MR, Saha SK (2008) Multi-resolution segmentation for object-based classification and accuracy assessment of land use/land cover classification using remotely sensed data. Journal of the Indian Society of Remote Sensing 36(2):189–201

Rees G (1999) The remote sensing data book. Cambridge University Press

Sarmap (2007) The SAR—guidebook. Sarmap

Singh SK, Srivastava PK, Gupta M, Thakur JK, Mukherjee S (2014) Appraisal of land use/land cover of mangrove forest ecosystem using support vector machine. Environ Earth Sci 71:2245–2255

Singh, S.K., P.K. Srivastava, S. Szabo, G.P. Petropoulos, M. Gupta & T. Islam (2016): Landscape transform and spatial metrics for mapping spatiotemporal land cover dynamics using Earth Observation datasets. Geocarto Int, 2016, pp1–16, doi:https://doi.org/10.1080/10106049.2015.1130084, 1

Sonka M, Hlavak V, Boyle R (1998) Image processing: analysis and machine vision. Second Revised Edition ed. Nelson Engineering

Srivastava PK, Han D, Rico-Ramirez MA, Bray M, Islam T (2012) Selection of classification techniques for land use/land cover change investigation. Adv Space Res 50:1250–1265

Srivastava PK, Mehta A, Gupta M, Singh SK, Islam T (2015) Assessing impact of climate change on Mundra mangrove forest ecosystem, Gulf of Kutch, western coast of India: a synergistic evaluation using remote sensing. Theor Appl Climatol 120:685–700

Srivastava PK, Singh SK, Petropoulos GP, Gupta M, Mukherjee S (2016) Landscape transform and spatial metrics for mapping spatio-temporal land cover dynamics using Earth Observation datasets. Geocarto Int:1–15. https://doi.org/10.1080/10106049.2015.1130084

Trimble (2013) eCognition Developer. [Online] Available at: http://www.ecognition.com/products/ecognition-developer [Accessed September 2017]

United States Geological Survey (2013) Landsat processing details. [Online] Available at: http://landsat.usgs.gov/Landsat_Processing_Details.php [Accessed Augustus 2017]

Whyte A, Fredinos K, Petropoulos GP (2018) A new synergistic approach for monitoring wetlands using sentinels -1 and 2 data with object-based machine learning algorithms. Environ Model Softw 104:40–57

Zhu Z, Woodcock CE, Olofsson P (2012) Continuous monitoring of forest disturbance using all available Landsat imagery. Remote Sens Environ 122:75–91